Design of dual-core optical fibers with NEMS functionality

Nina Podoliak*, Zhenggang Lian, Wei H. Loh, and Peter Horak

Optoelectronics Research Centre, University of Southampton, Southampton, SO17 1BJ, United Kingdom
*N.Podoliak@soton.ac.uk

Abstract: An optical fiber with nano-electromechanical functionality is presented. The fiber exhibits a suspended dual-core structure that allows for control of the optical properties via nanometer-range mechanical movements. We investigate electrostatic actuation achieved by applying a voltage to specially designed electrodes integrated in the cladding. Numerical and analytical calculations are preformed to optimize the fiber and electrode design. Based on this geometry an all-fiber optical switch is investigated; we find that optical switching of light between the two cores can be achieved in a 10 cm fiber with an operating voltage of 35 V.

OCIS codes: (060.4005) Microstructured fibers; (230.4685) Optical microelectromechanical devices; (060.2400) Fiber properties.

References and links

1. H.G. Craighead, "Nanoelectromechanical systems," Science **290**, 1532-1535 (2000).
2. P. F. Van Kessel, L. J. Hornbeck, R. E. Meier, and M. R. Douglass, "A MEMS-based projection display," Proc. IEEE **86**, 1687-1704 (1998).
3. M.C. Wu, O. Solgaard, and J.E. Ford, "Optical MEMS for lightwave communication," J. Lightw. Technol. **24**, 4433-4454 (2006).
4. V.T. Srikar and S.M. Spearing, "Material selection for microfabricated electrostatic actuators," Sens. Actuators A **102**, 279-285 (2003).
5. R. Moser, R. Wüthrich, L. Sache, T. Higuchi, and H. Bleuler, "Characterization of electrostatic glass actuators," J. Appl. Phys. **93**, 8945-8951 (2003).
6. F. Füzesi, A. Jornod, P. Thomann, M. D. Plimmer, G. Dudle, R. Moser, L. Sache, and H. Bleuler, "An electrostatic glass actuator for ultrahigh vacuum: A rotating light trap for continuous beams of laser-cooled atoms," Rev. Sci. Instrum. **78**, 103109 (2007).
7. B. Lenssen and Y. Bellouard, "Optically transparent glass micro-actuator fabricated by femtosecond laser exposure and chemical etching," Appl. Phys. Lett. **101**, 103503 (2012).
8. Z. G. Lian, X. Feng, P. Horak, L. Xiao, Y. Jeong, N. White, K. Frampton, J. A. Tucknott, H. Rutt, D. N. Payne, W. Stewart, and W. H. Loh, "Optical fiber with dual suspended submicron-cores," European Conference on Optical Communications (ECOC) 2011, 18-22 Sep. 2011, Geneva, Switzerland, paper Mo.2.LeCervin.1.
9. Z. Lian, P. Horak, X. Feng, L. Xiao, K. Frampton, N. White, J. A. Tucknott, H. Rutt, D. N. Payne, W. Stewart, and W. H. Loh, "Nanomechanical optical fiber," Opt. Express **20**, 29386-29394 (2012).
10. A. Butsch, C. Conti, F. Biancalana, and P. St. J. Russell, "Optomechanical self-channeling of light in a suspended planar dual-nanoweb waveguide," Phys. Rev. Lett. **108**, 741-755 (2012).
11. A. Butsch, M. S. Kang, T. G. Euser, J. R. Koehler, S. Rammler, R. Keding, and P. St.J. Russell, "Optomechanical nonlinearity in dual-nanoweb structure suspended inside capillary fiber," Phys. Rev. Lett. **109**, 183904 (2012).
12. Y. Akihama and K. Hane, "Single and multiple optical switches that use freestanding silicon nanowire waveguide couplers," Light Sci. Appl. **1,** e16 (2012).
13. M.W. Pruessner, K. Amarnath, M. Datta, D.P. Kelly, S. Kanakaraju, P.-T. Ho, and R. Ghodssi, "InP-based optical waveguide MEMS switches with evanescent coupling mechanism," J. Microelectromech. Syst. **14**, 1070-1081 (2005).
14. V. Kaajakari, *Practical MEMS*, (Small Gear Publishing, 2009).
15. M.M. Lee and M.C. Wu, "Tunable coupling regimes of silicon microdisk resonators using MEMS actuators," Opt. Express **14**, 4703-4712 (2006).
16. T. B. Jones, "Basic theory of dielectrophoresis and electrorotation," IEEE Eng. Med. Biol. Mag. **22**, 33-42 (2003).
17. T. B. Jones, *Electromechanics of Particles* (Cambridge University Press, 1995).

18. David J. Griffiths, *Introduction to Electrodynamics*, 3rd edition, (Prentice-Hall, 1999).
19. M. Bayindir, F. Sorin, A.F. Abouraddy, J. Viens, S.D. Hart, J.D. Joannopoulos, and Y. Fink, "Metal–insulator–semiconductor optoelectronic fibres," Nature **431**, 826-829 (2004).
20. M. Fokine, L. E. Nilsson, Å. Claesson, D. Berlemont, L. Kjellberg, L. Krummenacher, and W. Margulis, "Integrated fiber Mach–Zehnder interferometer for electro-optic switching," Opt. Lett. **27**, 1643-1645 (2002).
21. G. Chesini, C. M. B. Cordeiro, C. J. S. de Matos, M. Fokine, I. C. S. Carvalho, and J. C. Knight, "All-fiber devices based on photonic crystal fibers with integrated electrodes," Opt. Express **17**, 1660-1665 (2009).
22. P. J. A. Sazio, A. Amezcua-Correa, C. E. Finlayson, J. R. Hayes, T. J. Scheidemantel, N. F. Baril, B. R. Jackson, D.-J. Won, F. Zhang, E. R. Margine, V. Gopalan, V. H. Crespi, and J. V. Badding, "Microstructured optical fibers as high-pressure microfluidic reactors," Science **311**, 1583-1586 (2006).
23. K. Okamoto, *Fundamentals of Optical Waveguides*, 2nd edition (Elsevier/Academic Press, 2006).
24. P. Horak, W. Stewart, and W. H. Loh, "Continuously tunable optical buffer with a dual silicon waveguide design," Opt. Express **19**, 12456-12461 (2011).

1. Introduction

Optical systems with mechanically adjustable or controllable components are well known in the form of silicon chip based micro- and nano-electromechanical systems (MEMS and NEMS) [1] and are widely used in various optoelectronic devices for sensing, such as in accelerometers and gyroscopes, for 2-D optical switching in displays [2], and for a multitude of applications in optical communications [3]. While semiconductors are the standard material for the manufacturing of MEMS, the potential of glass-based materials for developing MEMS has also been investigated [4], and several groups have already demonstrated electrostatic glass actuators [5-7]. These developments open up the possibility of realizing equivalent electrically controlled mechanical systems based on glass optical fibers.

In a conventional telecommunication network optical fibers mainly transmit signals, while signal manipulation and switching are performed by separate devices that often require signal conversion from an optical to an electronic format. This leads to bulky and energy consuming circuits and it slows down the network performance. Realization of devices that allow for effective signal manipulation in the optical format would offer a huge advantage in the development of all-optical telecommunication networks. Further advantages could be obtained by integration of the active components into a fiber, combining transmission and control functionalities. Produced by fiber drawing techniques, dimensions of these active optical fiber components would not be restricted in comparison with chip based devices, which would facilitate some applications such as optical buffering. Moreover, such fiber devices would allow for low insertion loss and for easy integration with other components of all-fiber reconfigurable optical networks.

A reconfigurable nanomechanical optical fiber with a dual-core internal structure whose optical properties can be controlled through sub-micron mechanical movements has recently been demonstrated [8,9]. The fiber consists of two elliptical cores independently suspended by thin glass membranes in a central hole of a glass fiber of standard outer diameter. The supporting membranes are flexible, which allows the cores to move with respect to each other. The cores are separated by a small air gap, the size of which is comparable with the mode field diameter. The cores thus interact through their overlapping evanescent fields, forming a directional fiber coupler. The optical coupling length, and thus the fiber output, can be controlled very accurately by minute external forces giving rise to nanometer-size displacements of the cores, which can lead to a wide range of applications in the fields of sensing, switching, and all-optical network control. This first demonstration of an in-fiber nanomechanical switch was actuated by a variation of applied gas pressure [9], yet other actuation mechanisms could be envisaged in principle, such as stress, bending, and temperature. However, most of these methods are too slow for many applications, e.g. in telecommunication networks. Although sub-microsecond actuation of a nanostructured fiber was recently demonstrated using optomechanical forces [10,11], for most applications a more robust actuation method will be required.

We therefore focus here on an electrostatic actuation mechanism of the submicron cores in the dual-core fiber. Our system is thus the fiber equivalent of chip-based optical MEMS

switches based on two evanescently coupled waveguides as demonstrated recently for example in silicon [12] and InP [13]. Comb actuators are usually used for moving sub-micron sized guiding beams and waveguides on chips [14]. However, other methods have been recently introduced, including electrostatic actuation by means of a voltage applied directly to the waveguides [13] or by placing them in a non-uniform electric field created by nearby electrodes [15]. We demonstrate that the latter method gives a direct way to control light propagation in the dual-core fiber, leading to NEMS-type functionality in the system.

The paper is organized as follows. We start by analyzing how fiber optical properties depend on core dimensions in Sec. 2. In Sec. 3 we describe the electrostatic actuation method in a dual-core optical fiber with metallic wires integrated in the cladding. A simple analytical description of the electrostatic forces acting on the fiber cores is suggested and used to optimize electrode geometry in the fiber. The results are also compared to fully numerical finite-element simulations. Section 4 discusses the application of our proposed NEMS fiber as an all-fiber optical switch. We find that voltages as low as 35 V are required to achieve this operation. Finally, we conclude our discussions in Sec. 5.

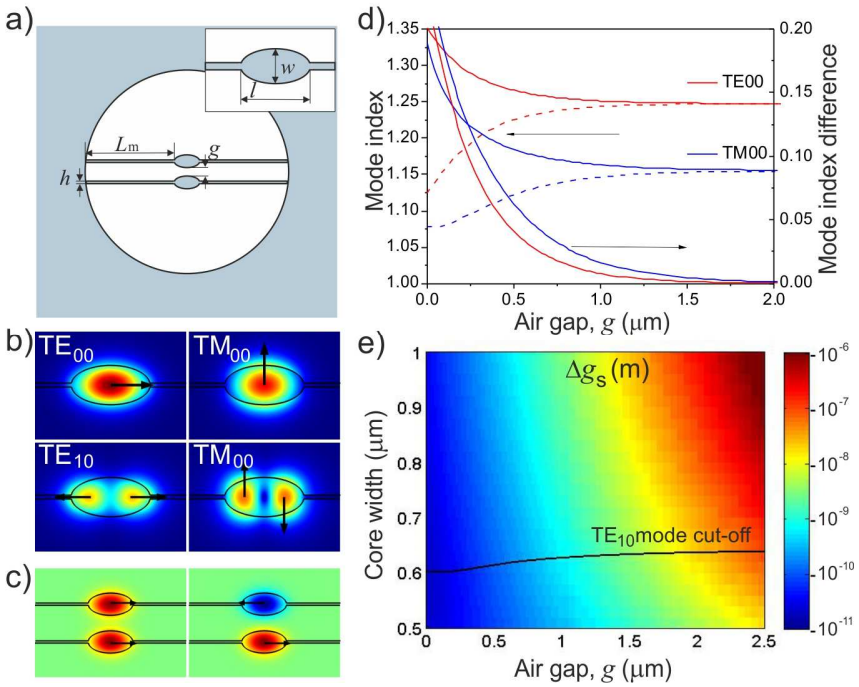

Fig. 1. (a) Schematic of the dual core fiber cross-section, where L_m and h are the membrane half-length and thickness, g is the air gap between the cores. Inset: l and w mark core length and width, respectively. (b) Electric field profile of hybrid TE and TM modes in a single core (colorplot: electric field amplitude normalized to the maximum of the TE00 mode; arrows: predominant electric field component polarization). (c) Symmetric and antisymmetric TE_{00} supermodes. (d) Effective mode indices of the TE_{00} and TM_{00} supermodes (solid and dashed lines correspond to symmetric and antisymmetric modes) and mode index difference between symmetric and antisymmetric modes of the dual core fiber with core size of 0.6×1.2 μm depending on the air gap between the cores. (e) Change of air gap Δg_s required to induce one optical switching cycle depending on core size and air gap for the TE_{00} mode; solid line shows cut-off of the higher order TE_{10} mode. In all calculations the material refractive index is 1.6, the wavelength is 1550 nm, the fiber length is 10 cm.

2. Modeling of the fiber

2.1 Optical mode structure

The concept of the dual-core optical fiber and its fabrication method have been presented previously [9]. In brief, the fiber has two elliptical cores that are independently suspended by thin flexible glass membranes and are separated by a small air gap, a cross section of which is schematically shown in Fig. 1(a). In this section we first analyze the fiber modal structure depending on the dimensions of the cores and the air gap between them. The optical modes supported by the fiber were numerically calculated by a full vectorial Finite Element Method (FEM) using Comsol Multiphysics®. In the model we assume a fiber made of lead silicate glass (Schott F2, refractive index n = 1.6) and a wavelength of 1550 nm. The core width was varied in the range from 0.5 to 1 µm, keeping the core aspect ratio (core length to width) fixed at 1.5, 2 or 2.5. The air gap was varied between 0 and 2.5 µm.

Analysis of the modal structure shows that an individual fiber core of size 1×2 µm supports four modes, see Fig. 1(b). Here we denote modes as TE/TM for predominantly horizontal/vertical polarization of the electric field component, although all modes are generally hybrid polarization modes. The lowest order TE_{00} and TM_{00} modes are mainly confined in the cores, while higher order modes are partly supported by the attached membranes leading to higher confinement losses. Therefore, we focus on the fundamental TE_{00} and TM_{00} modes in the following. For a core to support only the fundamental modes, its size should be smaller than 0.6×1.2 µm. By increasing the core aspect ratio, the higher order TE_{10} mode appears at a smaller core width; for example, for 1.5 and 2.5 core aspect ratios the core sizes for the higher mode cut-off are 0.7×1.1 µm and 0.5×1.3 µm, respectively.

In the following study we focus on a fiber which supports only the fundamental modes in the individual cores by fixing the core size to 0.6×1.2 µm. When the cores are placed close to each other, the individual core modes become coupled, forming symmetric and antisymmetric superposition modes, see Fig. 1(c). The effective mode indices of these supermodes depend on the coupling strength, and thus on the size of the air gap between the cores, as shown in Fig. 1(d). For other core dimensions in the studied parameter region a qualitatively similar behavior is found. The index difference between symmetric and antisymmetric modes (bottom curves) varies substantially with gap size (of order 10^{-3} for a few-nm variation) which allows for significant NEMS-type functionality, as demonstrated later in this paper.

The two fiber cores form a directional coupler. Thus, an optical signal launched into one of the cores will continuously switch between the cores while propagating along the fiber. The propagation distance at which the light transfers from one core to the other and back is given by the beat length of the supermodes

$$L_b = \frac{\lambda}{n_s - n_a}, \tag{1}$$

where λ is the light wavelength and n_s and n_a are the mode indices of the symmetric and antisymmetric supermodes, respectively. From Fig. 1(d) we find that L_b depends approximately exponentially on the air gap g.

Therefore, for a fiber of fixed length L and with light launched into one of the cores, a relative movement of the cores will lead to switching of the light between the cores at the fiber output. The required change of the air gap Δg_s to observe switching to the other core and back is approximately given by

$$\Delta g_s \approx \frac{L_b^2}{L\frac{\partial L_b}{\partial g}}. \tag{2}$$

Figure 1(e) shows Δg_s for switching of the TE_{00} mode on a logarithmic scale for a 10 cm long fiber for a range of core sizes and air gaps. It can be seen that for air gaps of order 1 µm a nanometer-range core movement will be sufficient for optical switching of light. We also note

from Eq. (2) that $\Delta g_s \propto 1/L$, meaning increased fiber sensitivity to core movement with an increase of its length.

In [9] switching was achieved experimentally through moving one core by 8 nm in a 43 cm long fiber at a core size of 0.8×2.7 µm. As seen in Fig. 1(e) for an increase of core size at fixed air gap, the modes become more localized in the cores and hence less coupled, requiring a large core displacement to observe optical switching. For significantly smaller core dimensions and air gaps, however, the fiber becomes sensitive even to sub-nanometer movements, making it unstable due to fundamental vibration noise. Thus for each core size an optimal air gap between the cores is found at which optical switching can be achieved with a realistic 1–10 nm core displacement, e.g. at around 1.5 µm for single-mode cores of 0.6×1.2 µm as discussed above.

2.2 Mechanical properties

The flexibility of the membranes connecting the cores to the fiber cladding allows for independent movements of the cores by an external force. The core displacement induced by a unit force per a unit fiber length, $\Delta g/F$, is entirely determined by the supporting membrane material and dimensions and can thus be tailored by optimizing the fiber design. By treating a membrane as a doubly clamped beam [14], from the classical Euler-Bernoulli beam equation we get:

$$\frac{\Delta g}{F} = \frac{1}{2E}\left(\frac{L_m}{h}\right)^3, \tag{3}$$

where L_m is the membrane half-length and h is its thickness, E is Young's modulus of the material. For example, for a membrane with $2L_m$ = 25 µm, and h = 0.1 µm, made of F2 glass (E = 57 GPa) we find $\Delta g/F = 17\times10^{-6}$ m^2/N, i.e. a force of 10^{-3} N/m can move a core by 17 nm. By making the membrane half as thick or twice as long, it is possible to increase the fiber mechanical response by almost an order of magnitude. The mechanical vibration frequency scales with the membrane size as $f \sim h/L_m^2$, but it also depends on the core dimensions, as having a large core with higher mass decreases the vibration frequency. For the previously reported fabricated range of fiber dimensions, the vibration frequencies were in the range of 0.5 – 10 MHz [8,9], thus suggesting mechanical response times of the fiber of the order of a few microseconds.

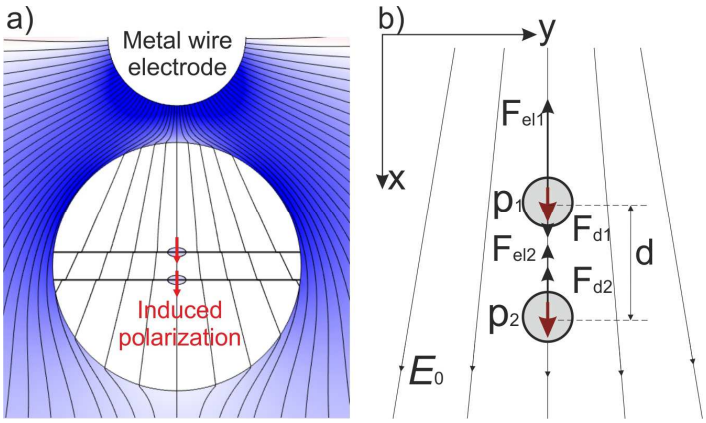

Fig. 2. (a) Electric field and induced material polarization of the dual core fiber in the vicinity of a metal wire electrode. The lines indicate the direction of the electric field. (b) Schematic of the analytical model showing the dielectrophoretic forces $\boldsymbol{F}_{el1}$ and $\boldsymbol{F}_{el2}$, and the dipole-dipole force $\boldsymbol{F}_{d1}$ and $\boldsymbol{F}_{d2}$ acting on the top and bottom dielectric cores, respectively, in the external electric field $\boldsymbol{E}_o$; d is the distance between the core centers.

3. Electrostatic actuation

As discussed above, the optical fiber properties can be modified by changing the size of the air gap between the two fiber cores. Here we investigate the possibility of electrostatic actuation of the cores by applying a static electric potential to one or more metallic wire electrodes embedded in the fiber cladding. This creates a non-uniform electric field around the electrodes, as shown schematically in Fig. 2(a), which polarizes the fiber material and creates forces pulling the cores towards the region of stronger electric fields. These forces are also known as *dielectrophoretic* forces, and are widely used to manipulate microparticles – such as cells, marker particles, etc. [16,17]. The dipole moments induced in the cores by the external field also give rise to a dipole-dipole interaction between the cores that becomes dominant over short distances, as we will demonstrate below.

3.1 Analytical description of dielectric forces

To understand the electrostatic mechanism of the fiber actuation and to optimize the electrode geometry, we first develop a simplified semi-analytical model. We describe the cores as two dielectric wires of circular cross section with radius r_0 and material dielectric permittivity ε placed at a distance d from each other in a non-uniform electric field $\boldsymbol{E}_0(\boldsymbol{r})$, see Fig. 2(b). Because the fiber length is significantly larger than the cross section dimensions, this system can be treated as a 2D problem. First, we evaluate the dielectrophoretic force acting on each core due to the external field gradient. The core is polarized by the external field, thus leading to an internal field of $\boldsymbol{E} = \boldsymbol{E}_0 + \boldsymbol{E}_{\text{in}}$, where the induced internal field in the 2D case is $\boldsymbol{E}_{\text{in}} = -\boldsymbol{P}/(2\varepsilon_0)$ [18]. The polarization $\boldsymbol{P}$ of the dielectric core is given by

$$\boldsymbol{P} = 2\varepsilon_0 \frac{\varepsilon - 1}{\varepsilon + 1} \boldsymbol{E}_0 . \tag{4}$$

Assuming that the core is small, so that the external field does not vary significantly over its cross-section, we calculate a core dipole moment per unit fiber length $\boldsymbol{p} = a\boldsymbol{P}$, where $a = \pi r_0^2$ is the core area. Then, the force acting on a dipole in the non-uniform electric field can be obtained as [16]:

$$\boldsymbol{F}_{el} = (\boldsymbol{p} \cdot \boldsymbol{\nabla})\boldsymbol{E}_0 = a\,\varepsilon_0 \frac{\varepsilon - 1}{\varepsilon + 1} \boldsymbol{\nabla} E_0^{\,2} . \tag{5}$$

If the same force is applied to the two individual cores of the fiber, they will move in parallel without changing their separation. We are thus interested in the *difference* between the dielectrophoretic forces $\boldsymbol{F}_{el1}$ and $\boldsymbol{F}_{el2}$ acting on the two cores separated by a distance d, see schematic in Fig. 2(b). By performing a series expansion over d, which is assumed to be small, the x-component of the force difference becomes proportional to the second spatial derivative of the field squared and to the distance between the cores:

$$\Delta F_{el} = F_{el1} - F_{el2} = a\,\varepsilon_0 d \frac{\varepsilon - 1}{\varepsilon + 1} \frac{\partial^2}{\partial x^2} E_0^{\,2} . \tag{6}$$

Next, we obtain an estimate for the dipole-dipole interaction between two dielectric cores having dipole moments $\boldsymbol{p}_1$ and $\boldsymbol{p}_2$ pointed in x-direction, Fig. 2(b). The electric field created by the dipole $\boldsymbol{p}_1$ at a distance $\boldsymbol{r}$ reads [18]

$$\boldsymbol{E}_1 = \frac{1}{2\pi\varepsilon_0} \left[\frac{2(\boldsymbol{r} \cdot \boldsymbol{p}_1)\boldsymbol{r}}{r^4} - \frac{\boldsymbol{p}_1}{r^2} \right]. \tag{7}$$

The force between two dipoles placed at a distance d can be calculated as the force acting on the dipole $\boldsymbol{p}_2$ in the field created by the dipole $\boldsymbol{p}_1$. The x-component of this force becomes

$$F_d = (\boldsymbol{p}_2 \cdot \boldsymbol{\nabla})E_1 = -\frac{1}{\pi\varepsilon_0} \frac{p_1 p_2}{d^3} \cong \frac{4a^2}{\pi} \varepsilon_0 \frac{(\varepsilon - 1)^2}{(\varepsilon + 1)^2} \frac{E_0^{\,2}}{d^3} . \tag{8}$$

Note that the attractive dipole-dipole force decreases as $1/d^3$ with increasing distance and thus will dominate for small air gaps over the induced forces, Eq. (6), that scale linearly with d.

As an example, we evaluate these forces in the fiber geometry of Fig. 2(a) where the non-uniform electric field $\boldsymbol{E}_0$ is created by applying a voltage V to a metallic wire electrode integrated into the fiber cladding. The electric field profile in the central air hole of the fiber (neglecting the cores and the supporting membranes) was calculated numerically for $V = 50$ V using the Electrostatic Module of COMSOL Multiphysics®, assuming a 27 μm sized air hole, and one electrode of 15 μm diameter placed at 25 μm distance from the air hole center. This numerically calculated field was then used in Eqs. (5) and (8) to calculate the forces $\boldsymbol{F}_{el}$ and $\boldsymbol{F}_d$ (shown by the dashed lines in Fig. 3), and hence the total forces acting on each dielectric core (solid lines) depending on the distance between their centers d, assuming that they are 1 μm in diameter and centered in the middle of the air hole. Note that the field strength $\boldsymbol{E}_0$ is directly proportional to the voltage V applied to the electrode, making both forces $\boldsymbol{F}_{el}$ and $\boldsymbol{F}_d$ proportional to V^2.

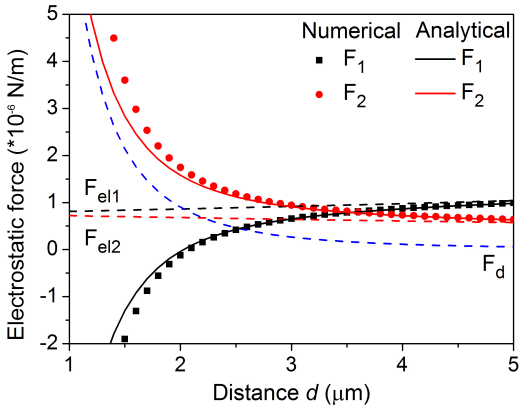

Fig. 3. Comparison between numerically (dots) and analytically calculated (lines) electrostatic forces acting on the circular dielectric cores of 1 μm diameter for a range of distances d between their centers, assuming the fiber geometry of Fig. 2(a), and 50 V voltage applied to the electrode. F_1 and F_2 are the total electrostatic forces, F_{el1} and F_{el2} are the dielectrophoretic forces acting on the top and bottom dielectric cores, respectively, and F_d is the attractive dipole-dipole force.

To validate our model, we compare these semi-analytical results to electrostatic forces calculated numerically by the FEM. The circular dielectric cores were added to the previous electrostatic model and the forces were calculated by numerical integration of the Maxwell surface stress tensor along the core boundaries for the same fiber geometry. The comparison between the electrostatic forces acting on each core for a range of distances between their centers is shown in Fig. 3. Excellent agreement between analytical and numerically calculated forces is observed at large distances between the cores. At these distances the total electrostatic force is determined mainly by the force $\boldsymbol{F}_{el}$, created by the external field gradient. This force pulls both cores in the same direction, towards the electrode, but with slightly different force magnitudes: the force $\boldsymbol{F}_{el1}$ acting on the top core in Fig. 2 (closer to the electrode) is larger than the force $\boldsymbol{F}_{el2}$ acting on the bottom core. So, for large gaps the relative force between the cores pulls them apart and the force magnitude increases linearly with increasing distance between the cores, as suggested by Eq. (6). For small distances, the total force is dominated by the attractive dipole-dipole interaction. As the distance decreases, there is a small deviation between the analytical and numerical results. This is attributed to the fact that in the analytical model we assumed an electric field created by a dipole in the form of Eq. (7). However, this formula is valid only at a distance larger than the dipole size. Hence, when the distance between the cores becomes comparable with the core size, the next order terms in $\boldsymbol{r}$ should be taken into account in Eq. (7).

3.2 Different electrode geometries

According to Eqs. (5) and (6), the forces acting on the individual cores and their relative movements are determined by the first and second spatial derivatives of the electric field, respectively. The field can be modified by introducing additional electrodes in the vicinity of the cores. A range of fiber geometries was therefore investigated, including configurations with one to four electrodes inside the fiber. These electrode geometries and the resulting electric field profiles $\boldsymbol{E}_0$ are shown in Fig. 4(a). The corresponding gradient and the second derivative of $|\boldsymbol{E}_0|^2$ inside the air hole are plotted in Figs. 4(b) and 4(c) as a function of the x coordinate ($y = 0$ here). In the fiber geometries with one and three electrodes, the gradient of $|\boldsymbol{E}_0|^2$ is always positive, suggesting that the two cores will be pulled by the dielectrophoretic forces in the same direction regardless of their position in the central air hole. In contrast, the gradient changes sign in the middle of the air hole in the cases of two and four electrodes and thus the dielectrophoretic forces act in opposite directions if the cores are placed at the center of the fiber. The geometries with three and four electrodes create larger field gradients than geometries with only one or two. However, the second derivative of $|\boldsymbol{E}_0|^2$ is hardly larger in the three-electrode case than in the two-electrode case at $x = 0$, suggesting only a small increase of the relative force between the cores, Eq. (6). The largest second derivative is achieved in the four-electrode configuration.

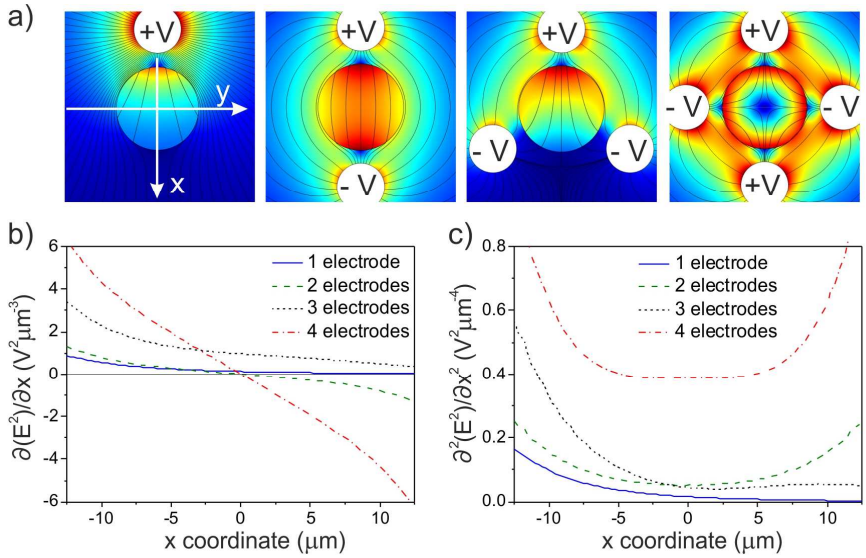

Fig. 4. (a) Different electrode geometries and their electric field distributions. Corresponding (b) ∇E_o^2 and (c) $\partial^2 E_o^2 / \partial x^2$ calculated inside the central air hole. In all calculations $V = 50$ V.

In order to achieve the largest field gradients, the metallic wire electrodes should be introduced in the vicinity of the optical cores. In our model we assumed a 4 µm separation between the electrode edge and the central air hole edge. In practice, the electrodes should be small enough not to distort the fiber core structure, but they must also be continuous to provide a uniform electric potential along the fiber. A multi-material co-draw technique to fabricate structural fibers with metal wires of a diameter below 10 µm was reported [19]. Alternatively it is possible to first draw the glass structure alone and subsequently fill the appropriate holes with metals by pressurizing melted alloy into the holes [20, 21] or by deposition of semiconductors and metals into them from chemical precursors [22].

Next, we use the electric field profiles and corresponding field gradients of Fig. 4 to calculate the forces acting on two circular glass cores of 1 µm diameter placed in the center of

the air hole following Eqs. (6) and (8). From these forces we can then evaluate the displacements of the cores relative to each other, i.e. the change of the air gap Δg, using Eq. (3) by assuming that the cores are suspended by ideal membranes which do not interact with the external field and introduce only elastic forces on the cores. The results Δg for the four geometries under consideration are shown in Fig. 5 as a function of the initial distance d between their core centers. Compared to the single-electrode configuration, a significant improvement in the relative core displacement at a small distance can be achieved in the two- and three-electrode geometries due to the higher dipole-dipole attraction between the cores. At large distances, where the interaction with the external field dominates, smaller improvements in the cases of two and three electrodes are observed that are related to the increase of the second order derivative of $|\boldsymbol{E}_0|^2$ as shown in Fig. 4(c). For each of the one-, two-, and three-electrode geometries an intermediate distance exists where the effects of the dielectrophoretic forces and the dipole-dipole forces cancel each other and no relative displacement of the cores is observed. The four-electrode configuration, on the other hand, leads to qualitatively and quantitatively different behavior. This geometry generates an electric quadrupole field with a vanishing field at the center of the fiber. Thus for small core separations, i.e. both cores sitting very close to the center, no dipole moments are induced and thus the dipole-dipole force also vanishes. The forces on the cores are therefore always dominated by the interaction of the individual cores with the background electric field leading to the approximately linear dependence on the core distance, as predicted by Eq. (6). The quadrupole field also exhibits the largest second derivative of $|\boldsymbol{E}_0|^2$, seen in Fig. 4(c), and thus the largest change of air gap of all geometries at the same voltage V for large d.

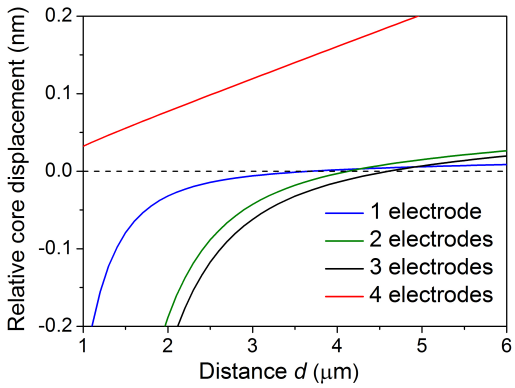

Fig. 5. Analytically calculated relative displacement Δg between two circular cores of 1 μm diameter depending on the distance between their centers for the fiber electrode configurations of Fig. 4(a). In all calculations V = 50 V. Positive and negative value of Δg corresponds to an increase and decrease of the air gap between the cores, respectively.

3.3 Fully numerical calculation

In the simplified semi-analytical model above we have neglected the influence of the supporting membranes on the electromagnetic field and on the induced forces. However, being made of the same material as the cores, the membranes can also be polarized and in this way create additional forces that influence the core displacements. Moreover, even if the membranes are much thinner than the cores, owing to their long lengths the membrane lateral cross-sections can be comparable to or even larger than the core areas with a correspondingly significant contribution to the forces. The induced polarization of one membrane will also create further complex interactions with the core electric dipoles and with the other membrane. Finally, all these induced fields and forces are distributed non-uniformly along the membranes, making a simple point-to-point approximation as in the previous section

impossible and also leading to membrane deformation profiles that differ from that of a classical doubly clamped beam.

To account for all these effects, we performed fully numerical FEM simulations using the MEMS Module of COMSOL Multiphysics® for the different fiber electrode configurations of Fig. 4. Here we assume elliptical cores of size 0.6×1.2 µm and supporting membranes of thickness 0.1 µm and length 25 µm. The model calculates the electrostatic forces acting on the cores and membranes as well as the structural deformations created by these forces. The calculated relative displacement of the cores for all electrode geometries depending on the initial distance between the core centers is shown in Fig. 6. Qualitatively, the behavior of the core displacement curves resembles the analytically calculated results in Fig. 5. However, the magnitude of the displacement in this case is much larger, especially at distances where the dielectrophoretic forces prevail. The distance range where these forces dominate also starts at a smaller separation between the cores. This suggests that the main difference between the numerical and analytical results is due to strong dielectrophoretic forces acting on the membranes because of the relatively large membrane cross-sections in this example (2.50 µm^2 compared with 0.57 µm^2 of a single core) while the dipole-dipole forces play a slightly smaller role. However all factors mentioned above contribute to the result.

In the one-electrode geometry with $V = 50$ V applied, the numerical model predicts relative core displacements of the order of ~ 0.1 nm that are probably too small for realistic in-fiber NEMS applications. The quadruple geometry, however, significantly increases the core displacements at distances > 1 µm. Relative core displacements greater than one nanometer are predicted in this case, which would be sufficient to introduce significant changes to the optical properties of the fiber as discussed in Sec. 2. An example application is discussed below in Sec. 4.

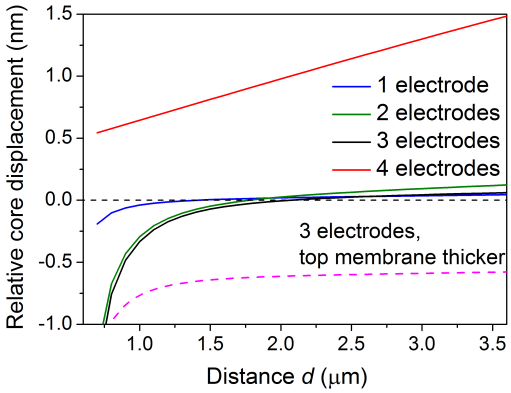

Fig. 6. FEM simulations of the relative core displacement depending on the distance between their centers for fibers with a core size of 0.6×1.2 µm and supporting membranes of 0.1 µm thickness and 25 µm length for the fiber electrode configurations of Fig. 4(a). Dashed line: top membrane thickness 0.2 µm. In all calculations $V = 50$ V.

Using the numerical model we also explore the possibility of changing the mechanical stiffness of the supporting membranes as another method for increasing the relative core displacement. For example, the dielectrophoretic forces acting on the cores in the three-electrode geometry are much higher than those in the one-electrode configuration, but they move both cores in the same direction and hence only give a small relative core displacement in a fiber with identical membranes. This can be mitigated if one of the supporting membranes is thicker than the other, so that similar forces introduce different displacements of the cores. To demonstrate this, we performed numerical simulations of a fiber where the top membrane is twice as thick as the bottom one. The relative core displacement in this case is shown in Fig. 6 by the dashed line; more than an order of magnitude improvement is demonstrated by this method.

4. Optical switching in a dual-core fiber using electrostatic actuation

As was shown in Sec. 2.1, moving the cores by as little as one nanometer can have a noticeable effect on optical fiber properties such as the beat length between the symmetric and antisymmetric supermodes. As an example, we describe an in-fiber optical switch with NEMS actuation based on the dual core fiber with the four-electrode geometry of Fig. 4. We consider a 10 cm long fiber with identical cores of 0.6×1.2 µm dimensions. Using the results of Fig. 1(e) an initial distance of 2 µm between the core centers is chosen (corresponding to a 1.4 µm air gap between them); at this distance a nanometer range core displacement is required to achieve optical switching. If a light beam is launched exclusively into a single core of the dual core fiber, it excites both symmetric and antisymmetric fundamental supermodes, and 100% switching of light between the cores can be expected if the cores are identical [23]. At the chosen fiber dimensions, the beat length for TE and TM modes is 735 µm and 263 µm, respectively, so a few hundred switching cycles occur along the fiber length. Varying the gap size changes the beat length of the coupled core modes and thus, depending on the applied electrode voltage, the output light can be switched continuously between the two cores. Figure 7 shows the predicted output intensity of one of the cores considering either TE or TM mode operation. In this configuration, a complete switch of the light from one core to the other can be achieved at ~ ±35 V for the TM_{00} mode and ~ ±55 V for the TE_{00} mode corresponding to a relative core displacement of 0.5 nm and 1.2 nm respectively. It should be noted that 100% switching of light can only be achieved if the two cores are identical. Having non-identical cores will decrease the switching contrast; experimentally an extinction ratio of 6 dB was observed previously due to a slight mismatch of the cores [9].

As already discussed in Sec. 2.2 the passive mechanical oscillation time of the membranes is of the order of about one microsecond in the under-damped regime. Faster switching could in principle be achieved by overdriving the system, that is, by applying an initial voltage spike to the electrodes to induce faster acceleration of the light-guiding cores towards their new position.

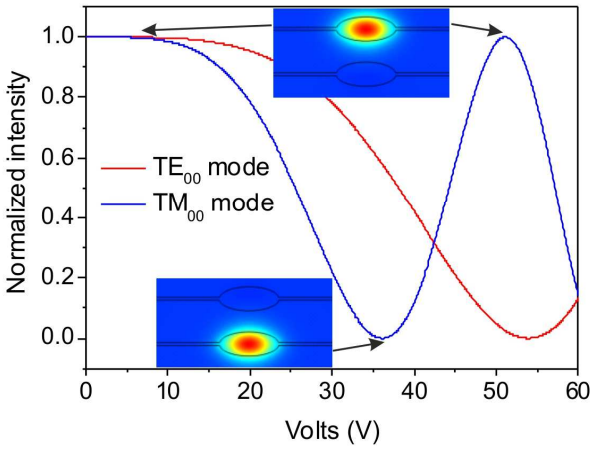

Fig. 7. Variation of the output intensity from one of the cores depending on applied voltage for a fiber with four-electrode geometry and with 0.6×1.2 µm core size and 2 µm initial distance between the cores. A fiber length of L = 10 cm was assumed. Insets: Mode fields of the switched output.

We finally want to comment on the dispersion characteristics of such an optical switch. Calculation of the group velocity dispersion from the data in Fig. 1 shows that the dispersion of the dual core fiber is of the order of -10^3 ps/nm/km and thus quite high compared to a standard step index fiber. Moreover the dispersion is highly dependent on the core size and the core to core separation: for the modeled fiber dimensions the dispersion changes by a

few ps/nm/km per 1 nm change of the core separation. However, noting that only a short piece of fiber is needed for optical switching (L = 10 cm in the example above), the total dispersion of the device would be of order 0.1 ps/nm and its variation during the switching operation of order 10^{-4} ps/nm, which would be negligible compared to other components in e.g. an optical telecommunications system.

5. Conclusions

We have investigated the possibility of electrostatic actuation of a dual suspended core fiber with NEMS-type functionality. The fiber core dimensions have been identified at which the fiber supports only fundamental modes but simultaneously exhibits significant modifications of its optical properties under nanometer-size mechanical re-configuration. For electrostatic actuation, metallic electrodes embedded in the fiber cladding are used to generate a non-uniform electric field inside the fiber. Interaction of the induced dipole moments within the optically guiding cores with this background field and dipole-dipole interaction between the two cores are identified as the dominant forces that lead to core actuation. A simplified semi-analytical model has been presented to analyze the parameter dependence of this mechanism and to investigate various electrode configurations. Of the investigated geometries, a quadrupole field generated inside the fiber by four electrodes was identified as the most promising design. Fully numerical FEM simulations have confirmed our analytical analysis.

Our results suggest that core displacements in the nanometer-range are feasible with this design, and are comparable with displacements recently demonstrated by a slow, macroscopic pressurization technique [9]. NEMS-type functionality with electrostatic actuation in such nanomechanical fibers thus looks promising. As an example application, we finally investigated optical switching between the two fiber cores based on our design and find that within a 10 cm length of fiber switching can be achieved with applied voltages of order 50 V. We expect this technology to open up the path towards a range of novel in-fiber applications such as tunable sensors, coherent beam steering, smart reconfigurable fibers, and optical buffering [24].

Acknowledgments

The authors thank Will Stewart for helpful discussions. We gratefully acknowledge financial support for this work from the Engineering and Physical Sciences Research Council via grant no. EP/J012874/1, the EPSRC Centre for Innovative Manufacturing in Photonics, and the “Photonic Hyperhighway” Programme Grant.